Sensors and Actuators B 232 (2016) 499–505

Sensors and Actuators B: Chemical

journal homepage: www.elsevier.com/locate/snb

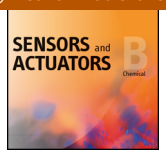

Permeation control in hydrogel-layered patterned PET membranes with defined switchable pore geometry – Experiments and numerical simulation

Adrian Ehrenhofer[a,*], Gert Bingel[b], Georgi Paschew[b], Marcus Tietze[b], Raoul Schröder[c], Andreas Richter[b], Thomas Wallmersperger[a]

[a] Institut für Festkörpermechanik, Technische Universität Dresden, 01062 Dresden, Germany
[b] Institut für Halbleiter- und Mikrosystemtechnik, Technische Universität Dresden, 01062 Dresden, Germany
[c] Bürkert Fluid Control Systems, Christian-Bürkert-Str. 13–17, 74653 Ingelfingen, Germany

ARTICLE INFO

Article history:
Received 7 January 2016
Received in revised form 18 March 2016
Accepted 29 March 2016
Available online 4 April 2016

Keywords:
Polymeric membranes
Finite element simulation
Hydrogel swelling
Microfluidics
Micromechanical pore valve
Particle separation

ABSTRACT

Permeation through polymeric membranes can be controlled by surface coating of a polyethylene terephthalate (PET) membrane with poly(N-isopropylacrylamide) (PNIPAAm) and inserting pores of defined geometry. When the temperature of the system rises above the volume phase transition temperature, the pores open, which allows permeation of formerly blocked particles. The exact control of the temperature allows defined change of the pore size and therefore enables separation abilities. Free swelling experiments are conducted to obtain the swelling behaviour of PNIPAAm. Then, a temperature expansion model is derived in order to simulate this behaviour with the finite element tool ABAQUS. The gained results are in excellent agreement with the observed shape change. Membranes with permeation control of particles can be used for biomedical application in microfluidics to analyse the size distribution of cells or in chemical information processing as a transistor-like component for an information-bearing chemical species. The possibility to simulate the behaviour of such permeation systems allows computer aided design and prediction of permeation abilities in these areas.

1. Introduction

Membranes are entities to separate compartments of different fluids. In biology, bilayer lipid membranes are self-assembling structures made of amphiphilic phospholipids. Embedded proteins allow specific permeation abilities for ions and molecules, which in some cases can be controlled by physical stimuli including electrical, chemical, mechanical and thermal signals. The underlying process is called gating [1].

In technology, membranes can be made of polymers with different porosity regarding their application area, e.g. filtration or reverse osmosis [2]. The technological equivalent of gating shall be called permeation control henceforth. Besides permeation control of ions and molecules, in life science, membranes for separation of particles with characteristic sizes in the sub-micron to micron range are of interest. Permeation control can be used in medicine to generate particle size profiles, e.g. in blood to analyse cells of anomalous size such as cancer cells. Another application area is the use as chemomechanical valves for flow control [3] or as transistor-like components for microfluidic integrated circuitries with a transistor circuit-based information processing concept [4].

In the present work, membranes with dynamically adjustable pore diameters and therefore tunable separation abilities controlled by temperature are introduced. Experimental results are given and the validity of the mechanical modelling with a temperature expansion model is shown. This allows the computer aided design of the filtration membranes with varying separation abilities.

Various research groups focus on porous polymer membranes made of stimuli responsive gels [5–9], where the permeation control is realised by a change in the hydrogel porosity. Further approaches use nanotubes [10–13] to achieve selective ion transport. The term *switchable gate membrane* [14,15] is also used for membranes which are surface functionalised to hinder transport parallel to the surface direction. Different groups have already used sensitive hydrogels for flow control [3] and as microfluidic valves [16]. Other research groups focus on the incorporation of

* Corresponding author.
E-mail addresses: adrian.ehrenhofer@tu-dresden.de (A. Ehrenhofer), andreas.richter7@tu-dresden.de (A. Richter), thomas.wallmersperger@tu-dresden.de (T. Wallmersperger).

http://dx.doi.org/10.1016/j.snb.2016.03.152

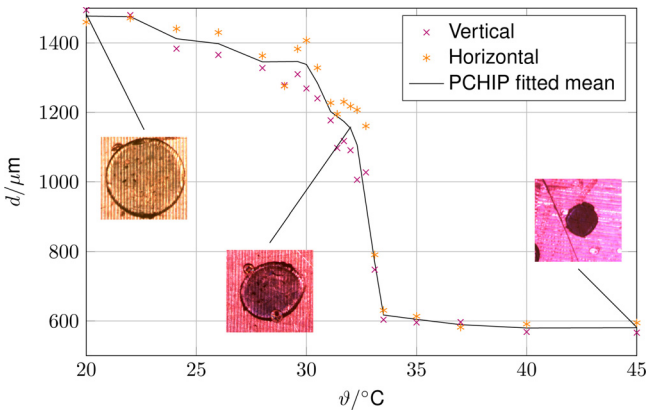

Fig. 1. Diameter of the disc versus temperature of a PNIPAAm sample. The mean value of the measurements is fitted with piecewise cubic Hermite interpolating polynomials (PCHIP).

biological membrane proteins into bilayer lipid membranes to achieve permeation control through natural gating mechanisms [17,18]. In the context of lab-on-a-chip devices, separation can be achieved in constant flow, e.g. by using branching [19] or capillary forces in microfilters [20].

The present work aims at a direct control of the permeation abilities. We demonstrate how permeation control membranes are designed, how the system can be characterised and how the properties of the smart actuator material can be transferred to a model of the experimental setup for numerical analysis. Therefore, the free swelling behaviour of the hydrogel poly(N-isopropylacrylamide) (PNIPAAm) is experimentally obtained (Section 2.1). A temperature expansion model for hydrogel swelling is derived in Section 2.2 and then implemented in a finite element tool to perform simulations. To verify the model, the free swelling behaviour of a simple model test setup is compared to the measured experimental values in this section as well. The design and the experiments of the switchable membrane are depicted in Sections 3.1 and 3.2; its numerical simulation is performed in Section 3.3. Additional information about the pore size evaluation from experimental microscopy results is given in Section 3.4. The results of the comparison between experiment and simulation for the complete permeation control system are depicted in Section 4. The conclusion is drawn in Section 5. Additional information is given in Appendix A.

2. Development of the material model

2.1. Free swelling behaviour of PNIPAAm

PNIPAAm shows lower critical solution temperature (LCST) behaviour. The swelling of the gel occurs due to the attracting chain interactions and the screening effect of water molecules (hydrohpilic interaction). For temperatures lower than LCST, the good screening properties of water molecules lead to a reduced interaction between the PNIPAAm chains, resulting in swelling. Those properties are lost when the temperature and subsequent movement/rotation of the water molecules increases over LCST. Then, there is a stronger attraction between PNIPAAm chains and the volume decreases, i.e. deswelling occurs. The process can be described as a first order volume phase transition [21].

To investigate the real swelling behaviour of the gel, a plate-like pad made of poly(N-isopropylacrylamide) is investigated under different temperatures (Fig. 1). At a temperature of 32 °C, the diameter is 1000 µm and the height is 120 µm. Below a temperature of 29 °C the PNIPAAm is completely swollen. Exceeding this temperature, the hydrogel collapses until it is completely shrunken at 35 °C. The experiments agree with the volume phase transition temperature of PNIPAAm in pure water [22], which is 32.8 °C.

Further information about the modelling background of the free swelling behaviour is given in Appendices A.1 and A.2. Image analysis is performed as described in Section 3.4. The pad diameter vs. temperature data is needed to calibrate the material behaviour with the temperature expansion model explained in Section 2.2.

2.2. Modelling and simulation of the thermal induced swelling of a PNIPAAm sample

The stress-free swelling of a hydrogel is assumed as an isotropic deformation. The underlying processes are given, e.g. by Attaran et al. [23] In the present work, we use a quasi-static temperature expansion model for the thermal swelling behaviour. Dynamic processes like temperature flux and locally varying strains are not taken into consideration in the present work. In contrast to other authors like Trinh et al. [24], our model is not an analogy for the chemical behaviour, but directly depicts the thermal volume expansion of the hydrogel as a linear-elastic material under varying temperature. In other works, the osmotic pressure derived from the ion distribution combined with a temperature dependent coefficient [25] is used to derive the swelling behaviour. The governing equations of the quasi-static thermo-mechanical problem are the mechanical balance equations

$$\sigma_{kl,k} + f_l = 0, \qquad \sigma_{kl} = \sigma_{lk} \tag{1}$$

the kinematics relation

$$\varepsilon_{kl} = \frac{1}{2}(u_{k,l} + u_{l,k}) \tag{2}$$

and the material law

$$\sigma_{kl} = E_{klmn}(\underbrace{\varepsilon_{mn} - \alpha \quad \delta_{mn} \quad \Delta\vartheta}_{\varepsilon^{el}_{mn}}) \tag{3}$$

where σ_{kl} is the stress tensor, f_l the volume load, ε_{kl} the strain tensor and E_{klmn} the tensor of elasticity. Please note that the equations are given in index notation for $k, l, m, n \in [x, y, z]$ and a summation over identical indices is performed (Einstein convention). $()_{,k}$ denotes the derivative in space with respect to the direction x_k. In the present case, there is no volume load, hence $f_l = 0$. The change of volume due to a temperature difference $\Delta\vartheta$ is defined through an isotropic strain with δ_{mn} being the Kronecker-Delta. In order to avoid buckling phenomena and allow superposition of thermal and mechanical strains, we use linear kinematics and the linear theory of elasticity, where the components of the strain tensor ε_{kl} are described via the gradients of the displacement u_k. For large deformations, the deformation gradient must be decomposed multiplicatively [26]. For a discussion about the linear and nonlinear approach, please see Appendix A.2. In the present form, the total strain ε_{kl} is gained by superposition of the thermal strain ε^{th}_{kl} and the elastic strain ε^{el}_{kl}

$$\varepsilon_{kl} = \varepsilon^{th}_{kl} + \varepsilon^{el}_{kl} \tag{4}$$

The elastic strain ε^{el}_{kl} is gained by the generalised Hooke's law (3) for linear isotropic deformation of a simple material. No viscous effects are considered, because the experiments are conducted in quasi-static condition, i.e. every point on the swelling curve (Fig. 1) is in thermal and chemical equilibrium.

To transform the swelling curve into an equivalent thermal expansion, the pad diameter, which describes the isotropic problem, is used. Preliminary studies on the analytical solution of the disc problem have proven that this approach is valid. Application of the pad area, which is not exactly circular due to manufacturing inaccuracies, instead of the mean diameter have proven to yield

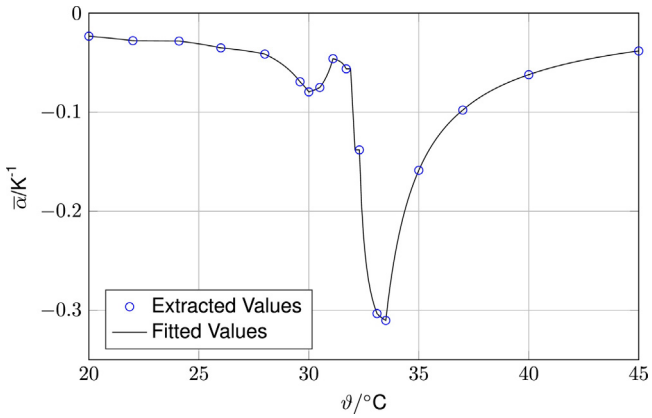

Fig. 2. Integral mean value of the thermal expansion coefficient $\bar{\alpha}(\vartheta)$ in reference to $\vartheta_{ref} = 32\,°C$. The extracted values are gained from the original measurements, while the fitted values use the strains from the PCHIP fitted mean values given in Fig. 1.

similar results (see Appendix A.1). The strain $\varepsilon^{\vartheta_{ref}}$ is calculated relating to the reference length $L_{ref} = L(\vartheta_{ref})$ at $\vartheta = \vartheta_{ref} = 32\,°C$. The integral mean value of the thermal expansion coefficient is

$$\bar{\alpha}(\vartheta) = \frac{\varepsilon^{\vartheta_{ref}}}{\vartheta - \vartheta_{ref}} \tag{5}$$

This value is gained for every data point from the experimental mean values (extracted values) and the piecewise cubic Hermite interpolation polynomial (PCHIP) fitted data points (fitted values) in Fig. 2. As the experimental measurement points and respective extracted values of α are much coarser, the fitted values are used for further simulation instead.

The material behaviour is implemented in the finite element tool ABAQUS for a disc of defined dimensions at reference temperature with diameter $d = 1000\,\mu m$ and height of $h = 120\,\mu m$. For the free swelling simulation, the disc is fixed at the middle and stress-free on the outer arc. The free swelling results in experiment and simulation are compared in Fig. 3. Excellent agreement between the measured ABAQUS output and the original swelling curve is observed, which proves the validity of the temperature expansion model.

3. Experimental and numerical investigations

3.1. Design of the permeation control membrane

The permeation control membrane is a hydrogel layered patterned polymeric membrane. It is based on a support membrane

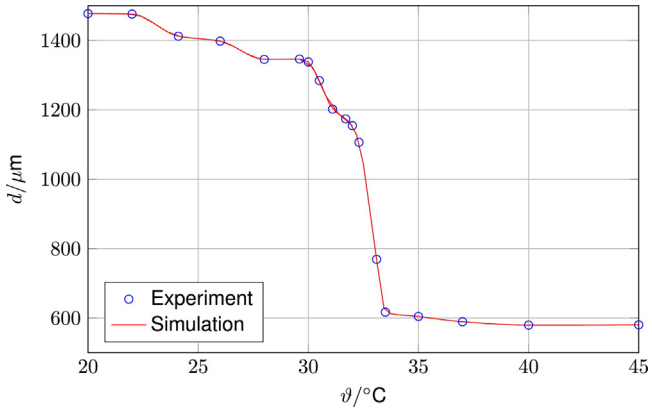

Fig. 3. Comparison of free swelling behaviour between experiment and numerical simulation.

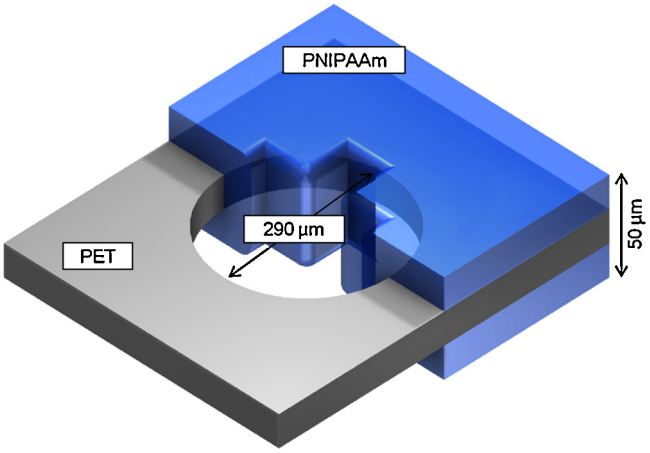

Fig. 4. Setup of the permeation control membrane consisting of a PET support membrane, which acts as a substrate for the PNIPAAm hydrogel layer.

made of polyethylene terephthalate (PET), which is layered with a poly(N-isopropylacrylamide) film [27]. Materials and preparation are described in Sections 3.2.1 and 3.2.2.

For achieving a robust and durable setup, a specific arrangement is chosen consisting of a support membrane incorporated in a stimuli-responsive material. The setup is displayed in Fig. 4. The geometrical form of the pore is important for both opening/closing abilities and the bypass stream obtained when the membrane pores are blocked by particles (fouling). In the present studies, a cross geometry is chosen. The cross geometry provides a large opening of the pore and a tight closing. Meanwhile, it allows a high bypass stream while granting good separation abilities and minimizing fouling problems. Further optimisation of the pore geometry can be achieved with numerical experiments described in this work.

3.2. Experimental investigations

After synthetisation of the system according to the recipe described in Section 3.2.1, measurements on the pore system for different temperatures were performed. To gain the free swelling behaviour of the hydrogel due to temperature stimulus which is needed for the numeric model calibration, cylindric samples were prepared according to Section 3.2.2. The microscopy images were taken as described in Section 3.2.3.

3.2.1. Materials and preparation of the permeation control membrane

The composite structure (Fig. 4) of the static polymeric support membrane and active hydrogel is created in several steps. The carrier material is a Mylar® foil.

Step 1. Into the substrate, the first circular holes with a diameter of $d = 290\,\mu m$ are cut by laser ablation.
Step 2. The material is activated for 60 min in an ozone-atmosphere produced under an UV-lamp.
Step 3. An adhesion promoter is applied. For this purpose, a 0.1 weight-percent solution of (3-methacryloyloxypropyl)dimethyl-chlorsilane in dicyclohexyl is applied for 1 h, thus creating covalent binding of methacryl-groups on the surface. Isopropanol is then used for cleaning of the surface and argon gas for dry-rinsing.
Step 4. The active material is polymerised and covalently bound on the surface. For this purpose, a reaction container is build which consists of two glass slides and spacers arranged such as to ensure that cavities exist at both sides of the foil. This results in both a constant height of the active material

and liquid layers at both sides. The reaction container is initially rinsed with protective gas (argon). Following, a pre-polymer solution is filled into the chamber which consists of 1.25 mol/l acrylamide-monomer, 1.5 mol% crosslinker N,N-methylenebis-(acrylamide) (BIS) and 1 mol% photoinitiator 2-hydroxy-4′-(2-hydroxyethoxy)-2-methylpropiophenone (98%) dissolved in deionised water. The solution is initially purged with argon for 30 min. UV polymerisation is carried out in an ice-bath under exposure of UV light (365 nm peak wavelength, 50 mW/cm^2, 120 s).

Step 5. The final shape of the pore is cut into the air-dried hydrogel by laser ablation.

3.2.2. Materials and preparation of the free swelling experiments

The same procedure as in Section 3.2.1 without the substrate foil is used to create the free swelling samples. Here, UV light is only locally applied using proximity lithography and a photo lithographic mask (TypoPhot TO-G). As a shape, small cylinders with a diameter of 1 mm and a height of 120 μm are chosen. The exposure time under UV light is 45 s.

3.2.3. Microscopy images

For the microscopy images of the permeation membrane system, the hydrogel composite foil is placed directly on an aluminium surface which is precisely adjusted in temperature by a Julabo F25 cryostat. To form a cavity with temperated swelling agent, a 200 μm spacer and a glass cover are arranged in a way that the composite foil is not in contact with the spacer or cover.

The temperature measurements are performed with a Qtemp 600 thermocouple device with an error of ±0.1 K. The equilibrating time after each change of temperature is 10 min. Preliminary studies have shown that in comparison to an equilibration time of 20 and 40 min, no difference in swelling degree could be observed. Between 23 °C and 27 °C the temperature steps are 2 K. Within the more sensitive region of 27 °C to 35 °C steps of 0.5 K are used. Above this temperature, 1 K steps are used. The diameter measurements are performed via image analysis. The scale is calibrated on a 20 mm normal. The microscope is of the type Leica WILD 450.

For the free swelling samples, which lack the support of the PET membrane, another experimental setup is used. To avoid tilting of the sample or sticking to the surface, the hydrogel pads are placed on a borosilicate glass sheet of 100 μm thickness and hold in place by a spacer. Here, a minimal equilibration time of 25 min is chosen for each temperature step to account for the increased thermal resistance and thus slower heat transfer through the borosilicate glass.

3.3. Numerical simulation of the permeation control membrane

The permeation control membrane is simulated with the finite element tool ABAQUS. Utilizing the symmetry of the pore, now only a quarter of the PNIPAAm structure embedded into the PET membrane is simulated. The structure is fixed at the outer arc, as the PET membrane has a much higher stiffness than the hydrogel. Symmetry boundary conditions are given at the inside of the hydrogel structure. Self-contact conditions are given for the edges and in respect to the symmetry planes to avoid intersection of the structure in the closed state. In Fig. 5, the finite-element model with mesh and boundary conditions is depicted.

Please note that preliminary studies with a circular disk, fixed at the outside with a circular opening (cylindrical pore), were conducted. In these studies and by analytical derivation it was proven, that the displacement is independent from the Young's modulus, but strongly depends on the Poisson's ratio.

For the simulation of a single pore structure in the membrane, linear three-dimensional solid elements are used to also obtain the height change via transversal contraction. 1380 hexahedral and 120 wedge elements are needed to obtain an adequate mesh for the simulations.

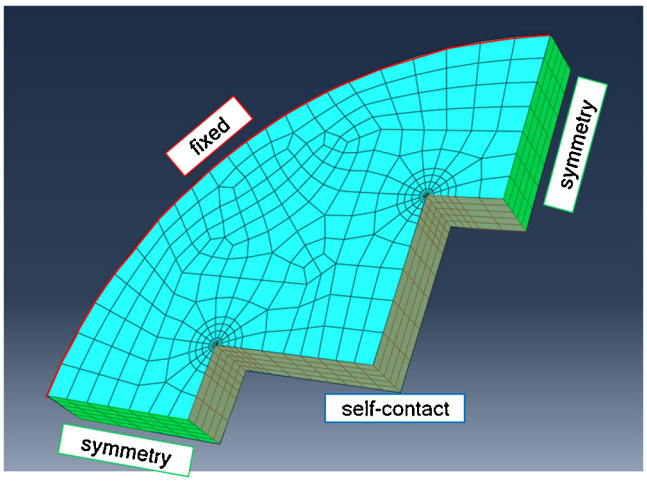

Fig. 5. Finite-element model of the quarter pore. The structure is fixed at the outer arc. Symmetry conditions are given at the top right and bottom left areas, while self-contact conditions and contact to the symmetry planes (analytical rigid planes) are given at the cross-flanks.

With the above derived temperature expansion model as temperature dependent expansion coefficient, numerical simulations are conducted to mirror the experiments and compare the implementation. Therefore, the dimensions acquired by image analysis of the pore geometry (see Section 3.4) are implemented.

The experiments are conducted on the equilibrium relation, i.e. for every measured state, thermal and chemical equilibrium is achieved, before the microscopy image is taken. The same is valid for the numerical simulations, where the model output is taken at every temperature step.

3.4. Image processing and evaluation of the geometry change

The starting point of the image evaluation is at the reference temperature $\vartheta_{ref} = 32\,^{\circ}C$. In this state, the pore geometry for the numerical simulation in ABAQUS is identified (Fig. 6). At each temperature, an averaging of the geometry values is realised, as the pore is not exactly symmetrical due to manufacturing inaccuracies. The measurements for gaining information about shape and opening/closing abilities are taken from image analysis of the microscopy images (Section 3.2.3) with the Open Source tool ImageJ, developed at the National Institute of Health.

The open area A at each temperature allowing water to pass as well as the hydraulic diameter $d_{hydr} = 4A/C$ with the circumference C of the cross-shaped pore are crucial for further investigation of the permeation abilities. The mean diagonal diameter d_{diag} is important for the size of the largest spherical particle that is able to pass the pore at a given temperature. The mean value from the north-west (NW) to the south-east (SE) edge and the south-west (SW) to the north-east (NE) edge is taken into account at each temperature. Thereby, the area blocked by a particle $A_{blocked} = \pi d_{diag}$ can be calculated.

When the pore is blocked, a water bypass occurs depending on the complementary area $A_{bypass} = A - A_{blocked}$. The second parameter to describe the shape of the pore in different opening or closing states to gain A is thus the mean normal diameter. It is taken as the mean in vertical direction north (N) to south (S) and horizontal direction west (W) to east (E). Comparing the normal and diagonal diameters in microscopy images and simulation outputs can give an insight, if the pore closing and opening is adequately simulated.

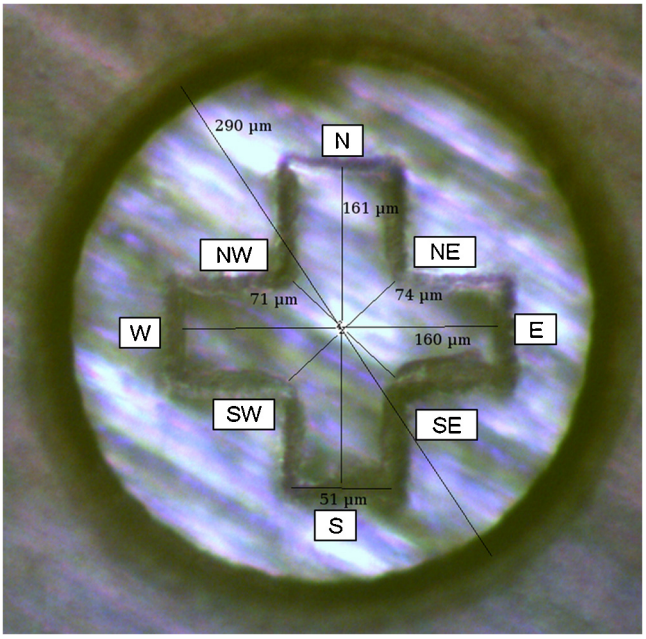

Fig. 6. Pore geometry in reference state at $\vartheta_{ref} = 32\,^{\circ}C$. The construction dimensions for the ABAQUS model were extracted from this picture with the Open Source tool ImageJ.

The interface between hydrogel and water is identified in the middle between the sharp colour transition and the distinguishable end of the hydrogel. The measurement error can thus be determined to about 5 pixels, with a scale of 4,975,750 pixels/m for the free swelling and 2,266,180 pixels/m for the pore system. This leads to an inaccuracy of ±2.21 µm for the free swelling and ±1.01 µm for the pore system. The discussion of the measurement errors and their propagation is done in Appendix A.3.

4. Results and discussion

Starting from the reference state at $\vartheta = (32 \pm 0.1)\,^{\circ}C$, the temperature is increased in steps of $\Delta\vartheta = 1\,K$ until full deswelling occurs at $\vartheta_{max} = 38\,^{\circ}C$ and the maximum pore diameter is reached. The temperature is then lowered to $\vartheta_{min} = 23\,^{\circ}C$ where the PNIPAAm is completely swollen and the pore is in a nearly closed state. Fig. 7 depicts the comparison between the diagonal diameter gained from the experiment through image processing (see Section 3.4) and

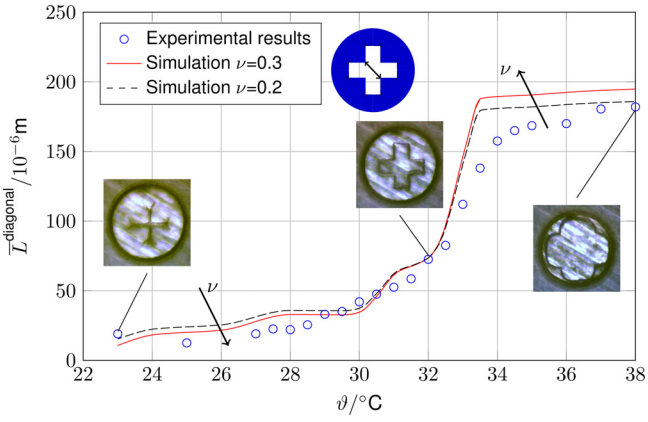

Fig. 7. Comparison of the mean diagonal diameter of the pore for different Poisson's ratios and the experimental results gained from image processing. The images were added for the closed state ($\vartheta = 23\,^{\circ}C$), the reference state ($\vartheta = 32\,^{\circ}C$) and the opened state ($\vartheta = 38\,^{\circ}C$).

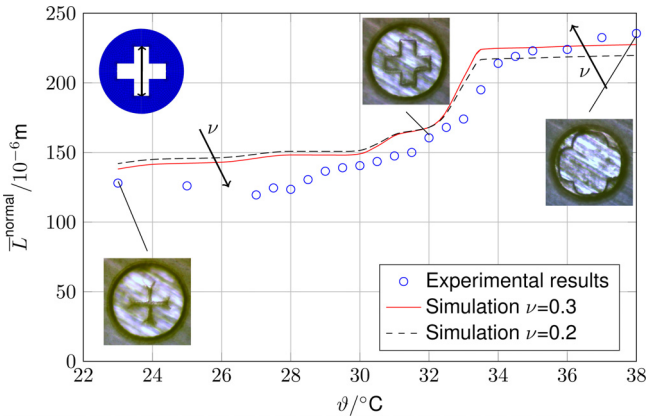

Fig. 8. Comparison of the mean normal diameter of the pore for different Poisson's ratios and the experimental results gained from image processing.

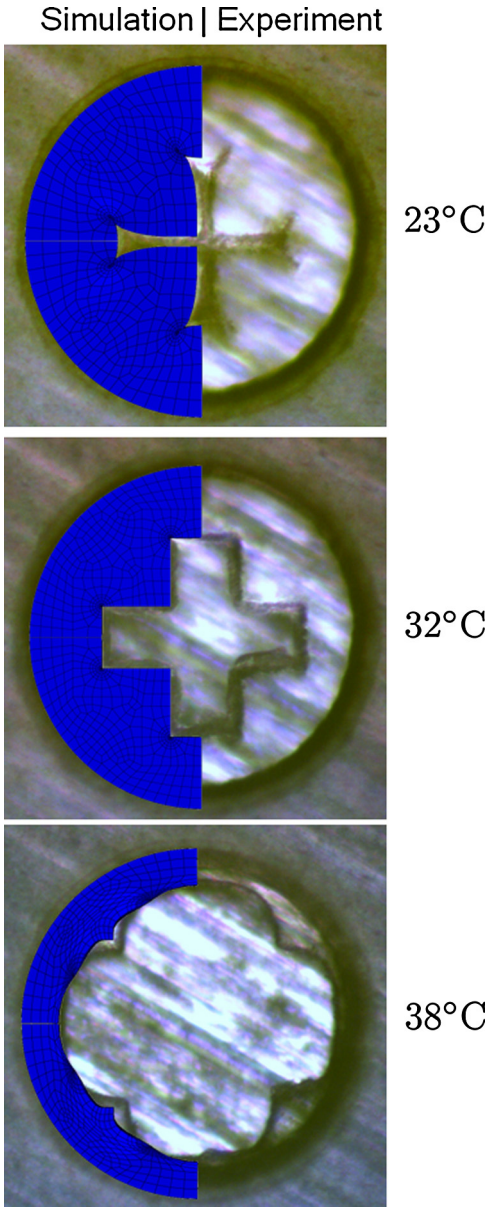

Fig. 9. Comparison of experimental images and simulation results for $\nu = 0.3$. The ABAQUS simulation output images are mirrored once to show the overall agreement with the microscope images of the half pore.

the numerical results gained from finite element simulation (see Section 2.2), which is important for the filtration performance, i.e. particles of which diameters are blocked. Different Poisson's ratios are assumed due to a lack of experimental and literature values. Preliminary analytical studies on the disc problem have shown, that the Young's modulus in this case plays no role in the deformation of the pore, but governs the corresponding stresses. Numerical simulations with the membrane pore system for very high and very low Young's moduli show the same behaviour. The normal diameter of the pore for different temperatures is depicted in Fig. 8.

The numerical simulation of the steady-state results are in excellent agreement with the experimental results, showing only small shape variations. A direct graphical comparison is drawn in Fig. 9, where the simulated quarter of the pore is mirrored once and overlaid to the experimental images. The difference between the images gained from experiment and the simulation are larger in opening, than in closing direction, starting from the reference temperature and the undeformed cross shape.

5. Conclusion

In the present work, we demonstrate that the quasi-static opening and closing behaviour of a hydrogel pore can be conveniently approached by a temperature expansion model and numerical simulation by using the finite element method.

The free swelling behaviour of the temperature-sensitive hydrogel PNIPAAm is used to calculate an integral mean expansion coefficient for implementation into the temperature expansion formula as stress-free volume expansion. Comparisons with a free swelling disk show an exact match in the measured points.

Temperature controlled opening and closing experiments with a cross-shaped pore are then conducted. The results are compared to numerical simulations of the setup with the before derived temperature expansion model. Different Poisson's ratios are used for calculation, each showing a slightly different geometry change. Overall, an excellent agreement between simulation and experiment is achieved.

This agreement allows the optimised design of pore membranes and pore-based microfluidic elements. The experimental setup is well adaptable to complex microfluidic integration and can serve different purposes, e.g. in biomedicine.

In further studies, our team aims at conducting both physical and numerical experiments to further analyse and refine the geometry of the pore. This will lead to better separation abilities and finer temperature control of the diameter. Additionally, first experiments with water flow through the pore will be conducted and used for comparison with the flow through the analysed shape. We will then bring in particles of defined varying size to proof the possibility of determining a size profile in continuous flow. An analytical flow model based on the Bernoulli equation will be used to predict this controllable separation behaviour. For physiological applications, the chemical composition of the PNIPAAm will be modified to better fit the temperature range of cells at the temperature of about 37 °C. As the swelling behaviour differs considerably when the transition temperature is shifted, a new material law will be derived for the biocompatible size profiling system.

This work is a first step to a computer-aided design of chemo-mechanical devices. It will allow the prediction of the behaviour of chemical circuitry analog to the Electronic Design Automation.

Acknowledgements

The present work is supported by funding of the Excellence Initiative by the German Federal and State Governments in the framework of the project 'Numerische und experimentelle Untersuchungen zur schaltbaren Permeabilität von Doppellipidschichten als intelligente Strukturen' at Technische Universität Dresden and partly by Bürkert Fluid Control Systems. It is also partly supported by the Research Training Group DFG-GRK 1865 "Hydrogel-based Microsystems" and by the Center for Advancing Electronics Dresden (cfaed) at Technische Universität Dresden.

Appendix A.

A.1. Comparison of one-, two- and three-dimensional swelling behaviour

When investigating the free swelling behaviour of a circular hydrogel disc, there are different possibilities to obtain the swelling degree. In its most simple form, we here use the diameter as a one-dimensional indicator for the strain and respective swelling degree. For manufacturing reasons, the hydrogel disc is not exactly circular but elliptic. Therefore, the mean diameter between minor and major axis is taken $\bar{d}^{1D} = (d^{\text{minor}} + d^{\text{major}})/2$. From image analysis, we can also obtain the area of the ellipse $A^{\text{ellipse}} = \frac{\pi}{4} d^{\text{minor}} d^{\text{major}}$ and calculate the diameter of a disc with equal area $\bar{d}^{2D} = \sqrt{d^{\text{minor}} d^{\text{major}}}$. The same can be achieved by measuring the three-dimensional volume change of the cylindrical body with elliptical base and calculating the volume of an equivalent cylinder, which needs a measurement in height-direction. In lack of height measurements of the hydrogel disc, only one-dimensional and two-dimensional mean values were compared. Only very small (<0.1%) differences in the resulting strain were detected. For the sake of easier error propagation calculation, the one-dimensional mean value was taken in consideration for future computations.

A.2. Discussion of nonlinear geometry (large displacement gradients)

When a hydrogel swells, it usually undergoes large displacements. For the simulations in this paper, small displacements are nevertheless used. This is due to two main reasons: At first, the implementation of the swelling behaviour uses discrete differences to obtain a temperature expansion coefficient. For every temperature step, ABAQUS uses the reference configuration (which is at 32 °C as in the derivation of the model) and the temperature difference to calculate the new element lengths. In this way, a perfect match between the model deformation and the experiments at the measured values is achieved (Fig. 2). For large deformations, instead of the discrete differences to the reference state, the local gradient of strain over temperature must be used. Nonlinear kinematics are then also needed in the definition of the expansion coefficient, i.e. α is obtained as the strain gradient over the temperature. The second reason is related to the mechanical behaviour at the edges. When the pore closes, the deformation leads to buckling problems at the edges of the cross-shape. They can be overcome by performing dynamic explicit simulations of the pore swelling or by post-buckling simulations. For dynamical simulations, the development of the temperature inside the structure must be simulated by solving the Poisson's problem of heat conduction. This more complex problem will be subject of future works.

A.3. Measurement errors and propagation

As mentioned above, the measurements in temperature have a random error of ±1 K. With the error in identifying the edges of the hydrogel of 5 pixels modified by their respective scale, a measurement error in length of ±2.21 μm and ±1.01 μm is obtained. Through Gaussian mean error propagation, we can calculate the

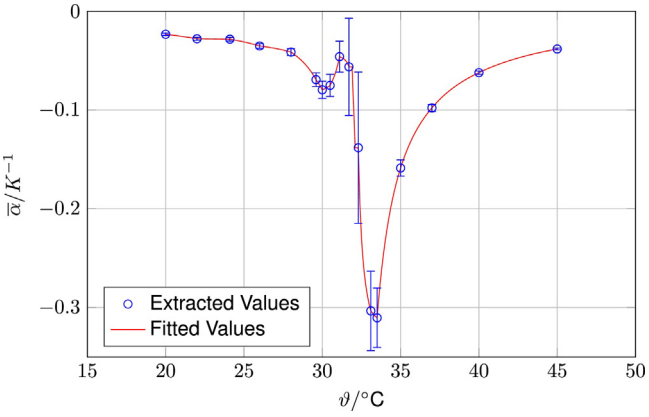

Fig. 10. Extracted errors of the mean integral expansion coefficient with error bars.

mean error for the swelling coefficient, which increases with smaller distance to the reference temperature (see Fig. 10).

References

[1] E. Gouaux, R. MacKinnon, Science 310 (2005) 1461–1465, http://dx.doi.org/10.1126/science.1113666.
[2] M. Ulbricht, Polymer 47 (2006) 2217–2262, http://dx.doi.org/10.1016/j.polymer.2006.01.084.
[3] K.-F. Arndt, D. Kuckling, A. Richter, Polym. Adv. Technol. 11 (2000) 496–505, http://dx.doi.org/10.1002/1099-1581(200008/12)11:8/12<496::AID-PAT996>3.0.CO;2-7.
[4] R. Greiner, M. Allerdissen, A. Voigt, A. Richter, Lab Chip 12 (2012) 5034–5044, http://dx.doi.org/10.1039/C2LC40617A.
[5] N. Adrus, M. Ulbricht, J. Mater. Chem. 22 (2012) 3088–3098, http://dx.doi.org/10.1039/C2JM15022K.
[6] S. Darvishmanesh, X. Qian, S.R. Wickramasinghe, Curr. Opin. Chem. Eng. 8 (2015) 98–104, http://dx.doi.org/10.1016/j.coche.2015.04.002.
[7] S. Frost, M. Ulbricht, J. Membr. Sci. 448 (2013) 1–11, http://dx.doi.org/10.1016/j.memsci.2013.07.036.
[8] Y. Ito, Y. Ochiai, Y.S. Park, Y. Imanishi, J. Am. Chem. Soc. 119 (1997) 1619–1623, http://dx.doi.org/10.1021/ja963418z.
[9] Y.S. Park, Y. Ito, Y. Imanishi, Langmuir 14 (1998) 910–914, http://dx.doi.org/10.1021/la970866r.
[10] F. Buyukserin, P. Kohli, M. Wirtz, C. Martin, Small 3 (2007) 266–270, http://dx.doi.org/10.1002/smll.200600477.
[11] H. Daiguji, Y. Oka, K. Shirono, Nano Lett. 5 (2005) 2274–2280, http://dx.doi.org/10.1021/nl051646y.
[12] S.B. Lee, C.R. Martin, Anal. Chem. 73 (2001) 768–775, http://dx.doi.org/10.1021/ac0008901.
[13] L. Wen, J. Ma, Y. Tian, J. Zhai, L. Jiang, Small 8 (2012) 838–842, http://dx.doi.org/10.1002/smll.201101661.
[14] P. Burgmayer, R.W. Murray, J. Am. Chem. Soc. 104 (1982) 6139–6140, http://dx.doi.org/10.1021/ja00386a061.
[15] Y. Liu, M. Zhao, D.E. Bergbreiter, R.M. Crooks, J. Am. Chem. Soc. 119 (1997) 8720–8721.
[16] A. Richter, D. Kuckling, S. Howitz, T. Gehring, K.-F. Arndt, J. Microelectromech. Syst. 12 (2003) 748–753, http://dx.doi.org/10.1109/JMEMS.2003.817898.
[17] A. Hirano-Iwata, M. Niwano, M. Sugawara, TrAC Trends Anal. Chem. 27 (2008) 512–520, http://dx.doi.org/10.1016/j.trac.2008.04.006.
[18] J.S. Najem, M.D. Dunlap, I.D. Rowe, E.C. Freeman, J.W. Grant, S. Sukharev, D.J. Leo, Sci. Rep. 5 (2015) 13726, http://dx.doi.org/10.1038/srep13726.
[19] M. Yamada, M. Seki, Lab Chip 5 (2005) 1233–1239, http://dx.doi.org/10.1039/B509386D.
[20] T.A. Crowley, V. Pizziconi, Lab Chip 5 (2005) 922–929, http://dx.doi.org/10.1039/B502930A.
[21] G. Gerlach, K.-F. Arndt, Hydrogel Sensors and Actuators: Engineering and Technology, vol. 6, Springer Science & Business Media, 2009.
[22] M. Andersson, A. Axelsson, G. Zacchi, J. Control. Release 50 (1998) 273–281, http://dx.doi.org/10.1016/S0168-3659(97)00151-X.
[23] A. Attaran, J. Brummund, T. Wallmersperger, Smart Mater. Struct. 24 (2015) 035021, http://dx.doi.org/10.1088/0964-1726/24/3/035021.
[24] Q.T. Trinh, G. Gerlach, J. Sorber, K.-F. Arndt, Sens. Actuators B: Chem. 117 (2006) 17–26, http://dx.doi.org/10.1016/j.snb.2005.10.041.
[25] K. Keller, T. Wallmersperger, B. Kröplin, M. Günther, G. Gerlach, Mech. Adv. Mater. Struct. 18 (2011) 511–523, http://dx.doi.org/10.1080/15376494.2011.605006.
[26] S. Galante, A. Lucantonio, P. Nardinocchi, Int. J. Non-Linear Mech. 51 (2013) 112–120, http://dx.doi.org/10.1016/j.ijnonlinmec.2013.01.005.
[27] A. Richter, G. Paschew, S. Klatt, J. Lienig, K.-F. Arndt, H.-J.P. Adler, Sensors 8 (2008) 561–581, http://dx.doi.org/10.3390/s8010561.

Biographies

Adrian Ehrenhofer (TU Dresden) started his research on the modelling and simulation of smart materials during his studies of mechanical engineering from 2009 to 2014. In 2014 he worked on the phenomenon of Backrelaxation in Ionic Polymer Metal Composites (IPMC) and on the modelling of membrane permeation in biological membranes with the multifield Poisson–Nernst–Planck approach. He is associate member in the Center for Advancing Electronics Dresden (cfaed) cluster of excellence and in the Research Training Group of the Deutsche Forschungsgemeinschaft GRK1865 Hydrogel-based microstructures. He currently works as a Ph.D. student at Technische Universität Dresden, Germany.

Thomas Wallmersperger (TU Dresden) is a full professor for Mechanics of Multifunctional Structures at TU Dresden. His research topics comprise coupled multi-field problems, adaptive materials and smart structures, discretisation and numerical modelling. Dr. Wallmersperger completed his dissertation (Ph.D. thesis) in 2003 and his habilitation in 2010 in Stuttgart, Germany. He has been a reviewer for multiple scientific journals, organizer of the "Second International Symposium on Design, Modeling and Experiments of Adaptive Structures and Smart Systems (DeMEASS II)" and of DeMEASS VII. Since 2009 he has been coordinator of the German–French doctoral school "Analysis of intelligent systems by considering multi-field couplings". Currently he is Associate Editor of the Journal of Intelligent Material Systems and Structures. Since 2000 Thomas Wallmersperger has published more than 80 conference and journal articles (h-index of 13 (Scopus)).